Emission wavelength variation with changes in excitation in a Re(I)/ bisthiazole ligand complex that breaks the Kasha-Vavilov rule

Kelly E. Henry,[a] Rebeca G. Balasingham,[b] Anthony R. Vortherms,[a] James A. Platts,[b] John F. Valliant,[c] Michael P. Coogan,[d*] Jon Zubieta[a*] and Robert P. Doyle[a*]

Supplementary Materials

Table of Contents

1. Experimental

1.1 Materials and Instrumentation

All chemicals, reagents, and solvents were purchased from Sigma-Aldrich, Alfa Aesar, or Fisher Scientific (USA) and used without further purification. An Agilent 1200 reverse-phase High-Performance Liquid Chromatography (HPLC) instrument with a manual injector and automated fraction collector was used for all purifications. An Eclipse C18 XBD analytical column (5 μm x 4.6 mm x 150 mm) was used for all purifications. All methods were run at a flow rate of 1 $mL{\cdot}min^{-1}$ at a UV detection of 254 nm. ^{1}H-NMR spectroscopy was conducted using a Bruker Advance DPX 500 MHz spectrometer. Mass

spectra were obtained using a Bruker Autoflex III Matrix-Assisted Laser Desorption/Ionization Time of Flight Mass Spectrometer (MALDI-ToF MS) or a Shimadzu 2000 Electrospray Ionization Mass Spectrometer (ESI-MS). Electron absorption spectra (EAS) were obtained using a Cary 50 UV-Vis spectrophotometer. Fluorescence spectra were obtained using a FluoroMax-4 spectrofluorimeter in HPLC-grade solvents, or on a JobinYvon-Horiba Fluorolog spectrometer fitted with a JY TBX picosecond photodetection module, with automatic correction of spectra for variations in instrument sensitivity with wavelength using the DataStation suite of software. Steady state spectra were recorded using a CW xenon excitation lamp with a single monochromator with excitation slits set to 2 nm. The sample chamber was arranged for orthogonal detection with 1 cm quartz cuvettes. Emitted light was passed through a single monochromator with emission slits set between 2 and 6 nm, and recorded on a 1911F emission signal detector. Luminescence lifetimes were obtained using either 295 nm or 372 nm nanoLEDs operating at 1 MHz. All lifetime data were collected using the JY-Horiba FluoroHub single photon counting module in multi-channel scaler mode and lifetimes determined using the provided decay analysis software package, DAS v6.1. Quantum yield measurements were obtained with aerated acetonitrile solutions, using $[Ru(bpy)_3](PF_6)_2$ (recrystallised from acetone/water mixtures at least three times) in aerated acetonitrile as a standard ($\Phi_{em} = 0.016$) with manual titration of samples to equal absorbencies and integration of emission areas using the facility provided in the DataStation suite of software.

DFT studies were carried out using Gaussian03[1] and Gaussian09[2] software. Initial geometry optimisation of **3'** and **N-Me 3'** (in its N,N, N,S and S,S forms) was

performed at the B3LYP/LANL2DZ[3][4] level in Gaussian03. Subsequent TD-DFT and energy comparisons also employed B3LYP, this time with a basis set consisting of 6-31+G(d,p)[5] on all atoms except Re, for which the Stuttgart-Dresden basis set and effective core potential[6] was used. Geometry optimisation and comparison of energy of configurations were done in gas phase, while TD-DFT calculations of absorption and emission energy employed the Polarizable Continuum Model (PCM) approximation of solvents.[7

1.2 Synthesis of 1,1-bisthiazole-(1,4)-diaminobutane (**3**)

N-Boc-1,4-butanediamine (300 mg, 1.5 mmol), and thiazole-4-carboxaldehyde (360 mg, 3.0 mmol) were mixed in anhydrous dichloroethane (DCE) (5.0 mL) under N_2 at room temperature for 30 min. Sodium triacetoxyborohydride (636 mg, 3.0 mmol) was subsequently added to the mixture along with an additional 5 mL of anhydrous DCE and the reaction was stirred for 16 h. After reaction completion, the solvent was removed under vacuum and the product was dissolved in 10% methanol (MeOH), 10% trifluoroacetic acid (TFA) (v/v) in H_2O and stirred for 3 h. The reaction was purified by reverse-phase HPLC, with a gradient of 100% 0.1% TFA in H_2O increased to 20% acetonitrile (MeCN) over 5 minutes, and increased to 40% MeCN over 2.5 minutes, and increased to 100% MeCN over 2.5 minutes. Yield is 10% at >95% purity, ^{1}H-NMR (500 MHz) D_2O: δ = 9.05 (s, 2H), δ = 7.81 (s, 2H), δ = 4.54 (s, 4H), δ = 3.28 (t, 2H), δ = 2.98 (t, 2H), δ = 1.87 (m, 2H), δ = 1.63 (m, 2H)

1.3 Synthesis of $Re(H_2O)_3(CO)_3Br$ (**5**)

$Re(CO)_5Br$ (9 g, 22.0 mmol) was dissolved in 100 mL dH_2O and refluxed at >100 °C for 24 h. The crude mixture was cooled to room temperature and filtered through a plug of Celite and the resulting product was concentrated under vacuum to give a light green powder. Yield was 90%.

1.4 Synthesis of [$Re(CO)_3$-1,1-bisthiazole-(1,4)-diaminobutane)] bromide (**3'**)

$Re(CO)_3(H_2O)_3Br$ (420 mg, 1.04 mmol), and 1,1-bisthiazole-1,4-diaminobutane (294 mg, 1.04 mmol) were refluxed in MeOH at >65 °C for 3 h. The solvent was reduced under vacuum and dissolved in 10% MeOH, 10% dimethyl sulfoxide (DMSO) (v/v) in H_2O. **3'** was purified by reverse-phase HPLC with a gradient of 95% 0.1 % TFA in H_2O and 5% MeCN increased to 12% MeCN over 7 minutes, then increased to 20% MeCN over 2 minutes, and finally increased to 25% MeCN over 5 minutes. The complex was characterized using MALDI-ToF MS using a 10 mg/mL alpha-cyano-4-hydroxycinnamic acid (CHCA) matrix, dissolved in 50:50 mixture of H_2O:MeCN with 0.1% TFA; **3'** was also characterized using ^{1}H-NMR in DMSO-d_6. Further characterization was done by EAS and fluorescence spectroscopy. Yield is 5% at >99+% purity based on HPLC (see Figure S5 t_R= 13 min). ^{1}H-NMR (500 MHz) D_2O: δ = 10.43 (d, 2H), δ = 8.61 (s, 2H), δ = 5.50 (m, 4H), δ = 3.82 (t, 2H), δ = 3.51 (t, 2H), δ = 2.82 (d, 2H), δ = 2.57 (t, 2H).

2. **Characterization**

*2.1 Characterization of **3***

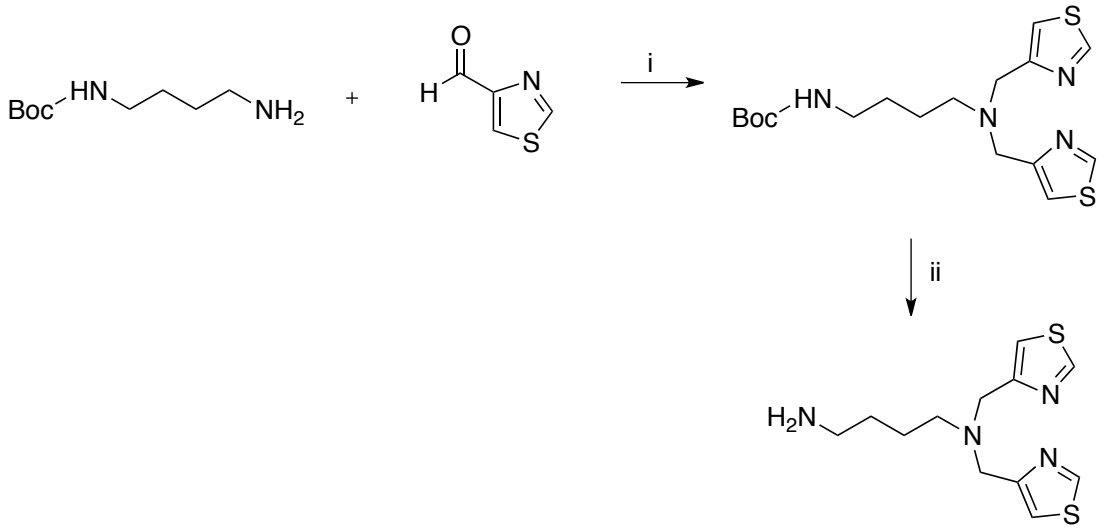

Scheme S1. Synthesis of **3**. Reaction conditions i: $NaBH(COOCH_3)_3$, anhydrous DCE, 16 h under N_2; ii: 10% TFA, 10% MeOH in H_2O, 3 h.

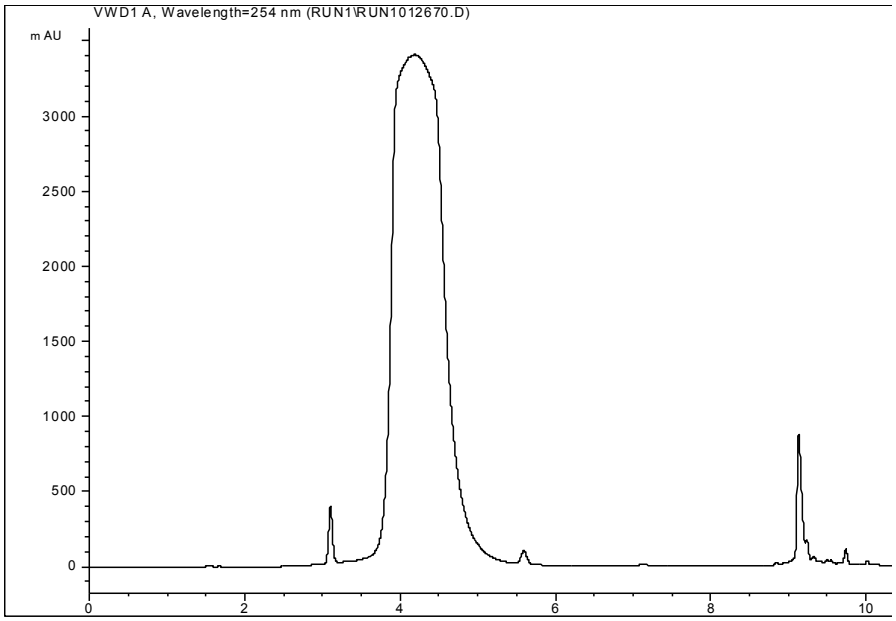

Figure S1. HPLC chromatogram of **3**; the peak at t_R 4.3 minutes was isolated and represents **3** as shown by ESI-MS and ^{1}H-NMR.

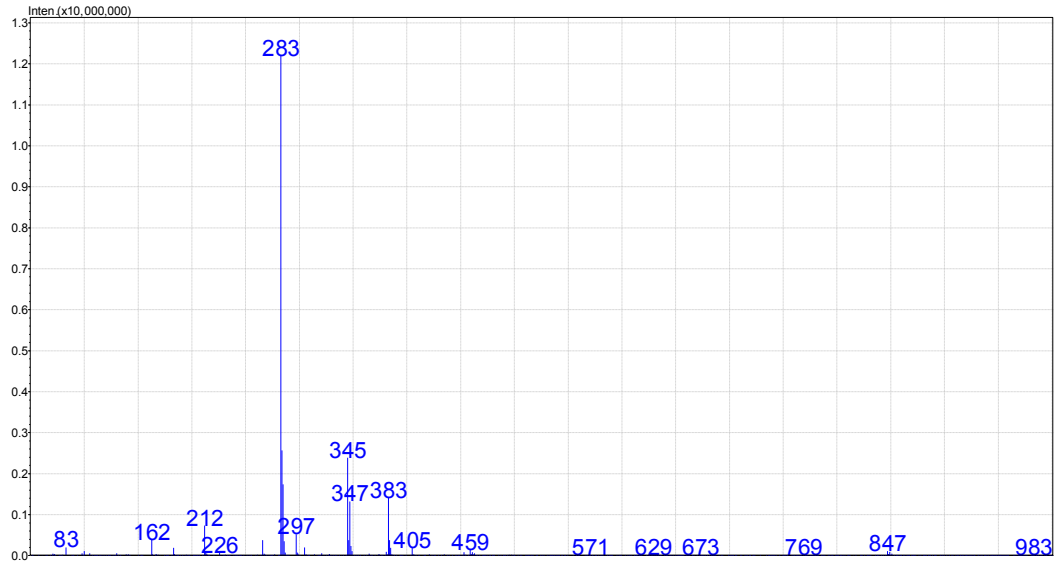

Figure S2. ESI-MS of **3**. Peak at 283 represents the predicted m/z for **3**.

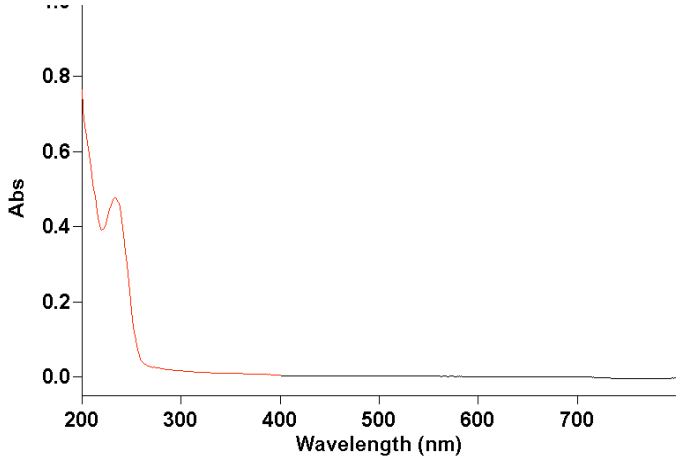

Figure S3. Electron absorption spectrum of **3**. The λ_{max} value is 235 nm.

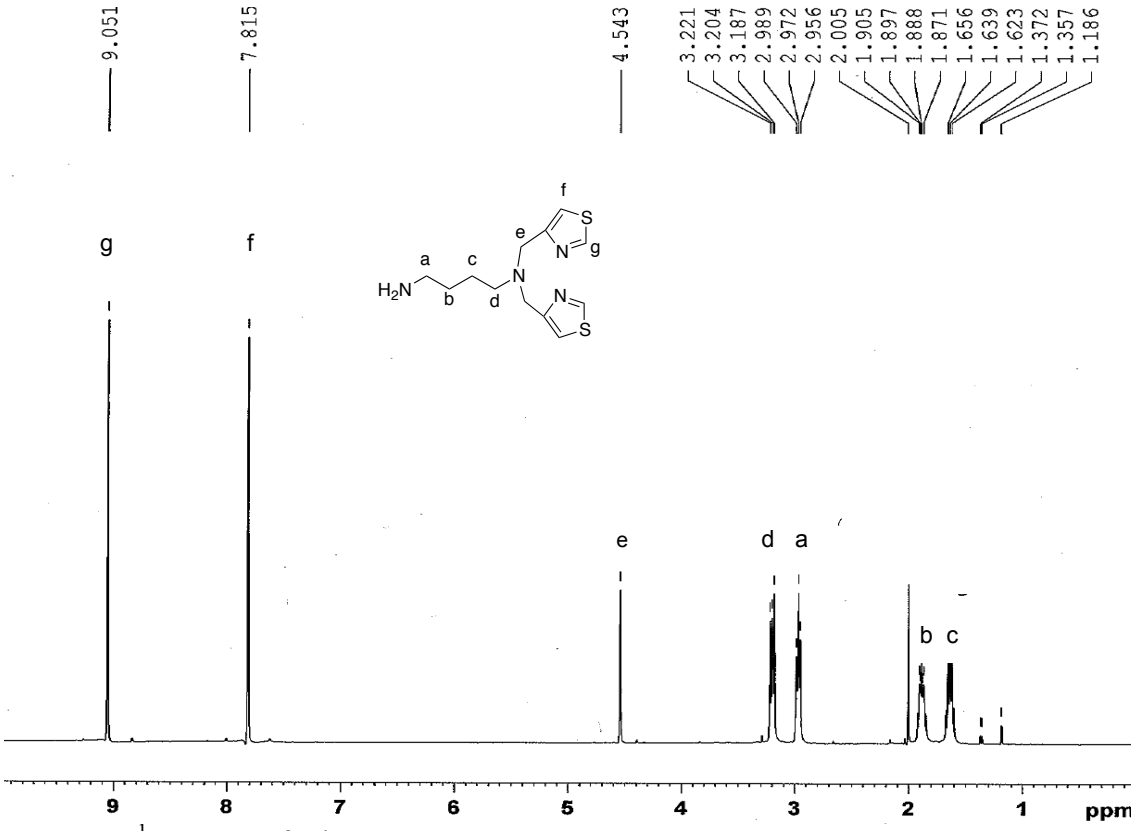

Figure S4. ^{1}H-NMR of **3** in D_2O.

*2.2 Characterization of **3'***

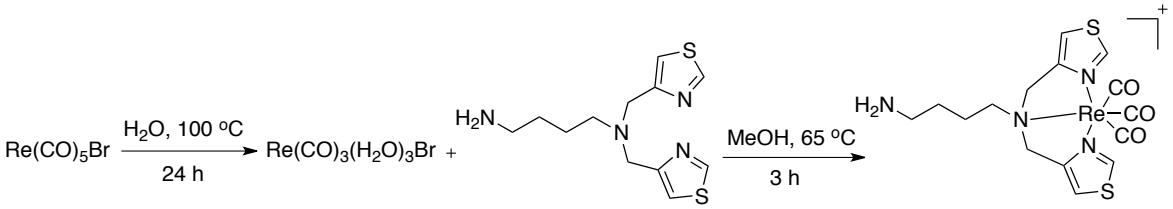

Scheme S2. Synthetic route to **3'**.

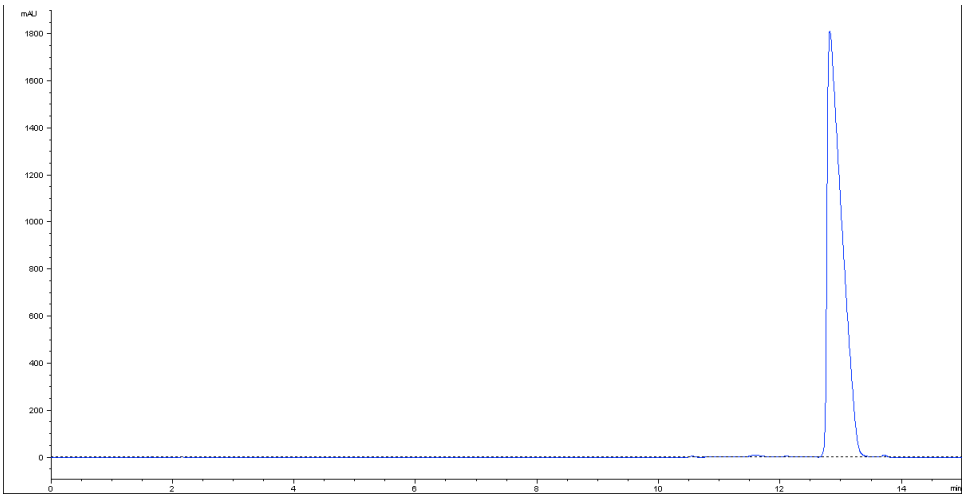

Figure S5. Chromatogram of **3'**; the peak at t_R 13 minutes represents complex **3'**. This peak was individually isolated and utilized in all subsequent photophysical studies.

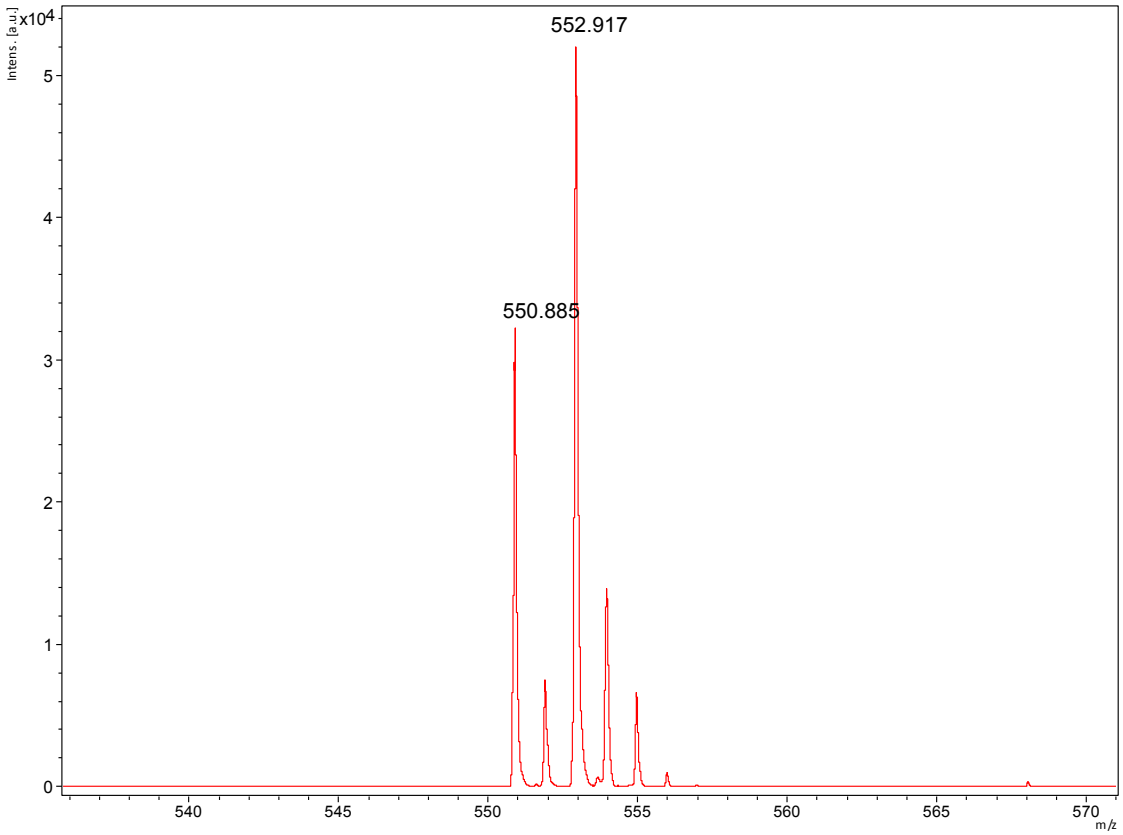

Figure S6. MALDI-ToF mass spectrum of **3'**. Peak at m/z 553 showing expected mass of complex **3'**, with the predicted isotopic distribution.

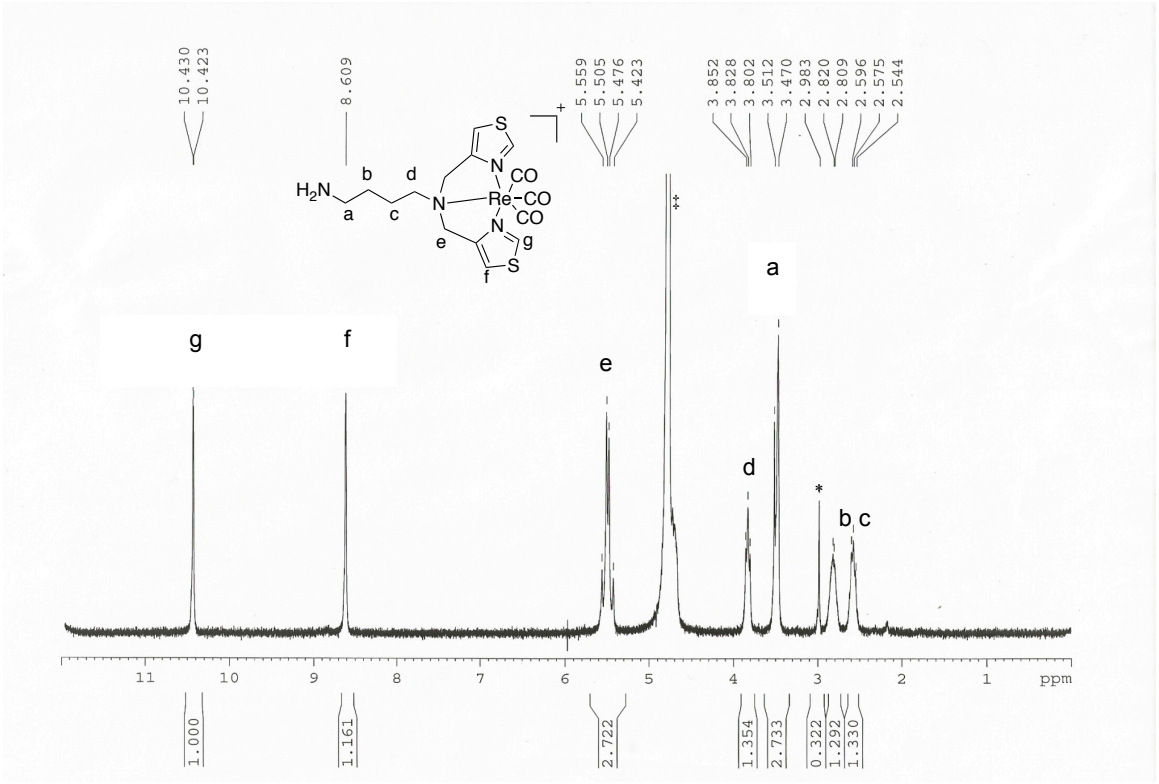

Figure S7. ^{1}H-NMR of **3'** in DMSO-d_6. ‡ represents HDO and * represents DMSO-Hd_5 present as solvent impurities.

*2.3 Additional Photophysical Data for **3'***

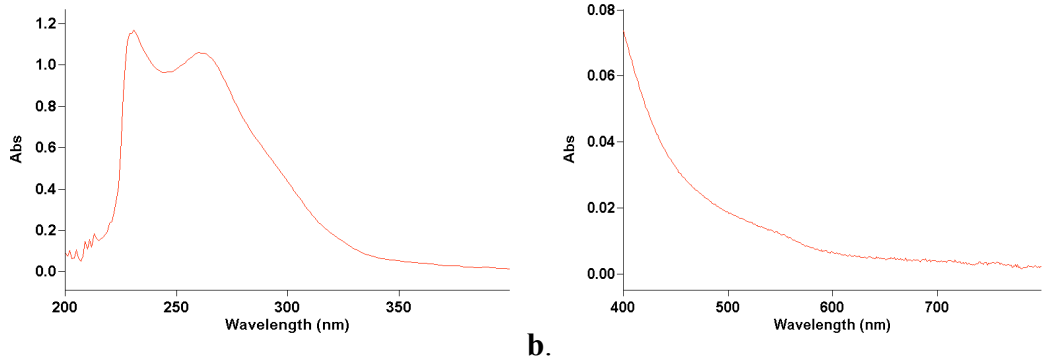

a. **b**.

Figure S8. Electron absorption spectrum of **3'** in MeOH. Separate scans were ran for the UV (**a**) and the visible (**b**) region.

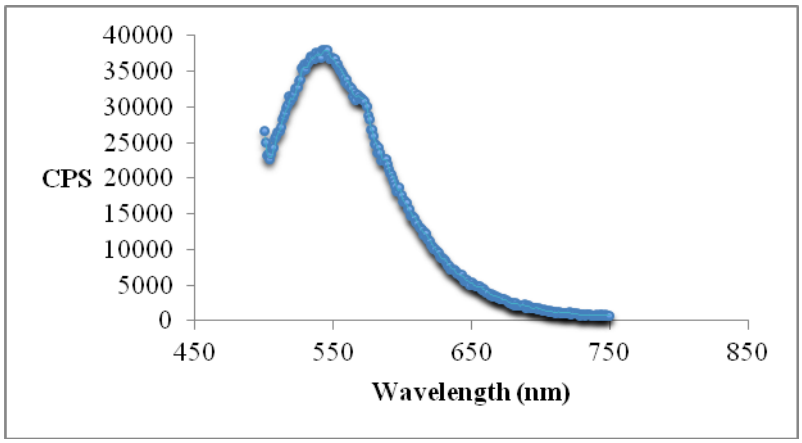

Figure S9. Emission spectrum of **3'** in MeOH via excitation at 488 nm.

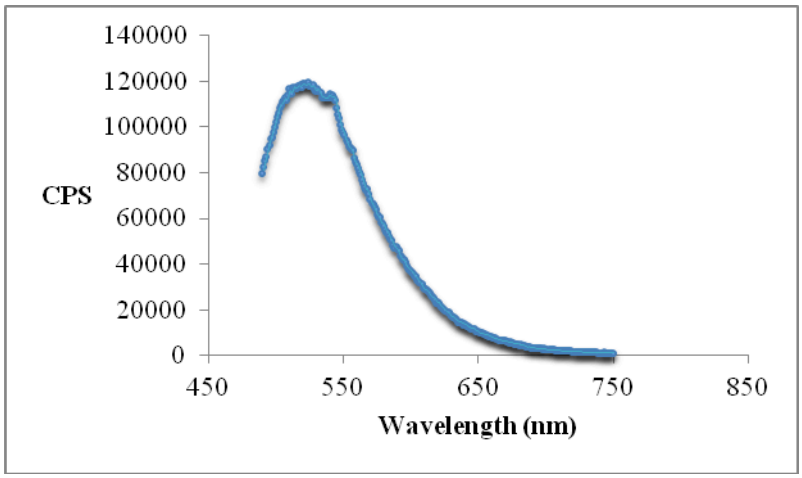

Figure S10. Emission spectrum of **3'** in MeOH via excitation at 468 nm.

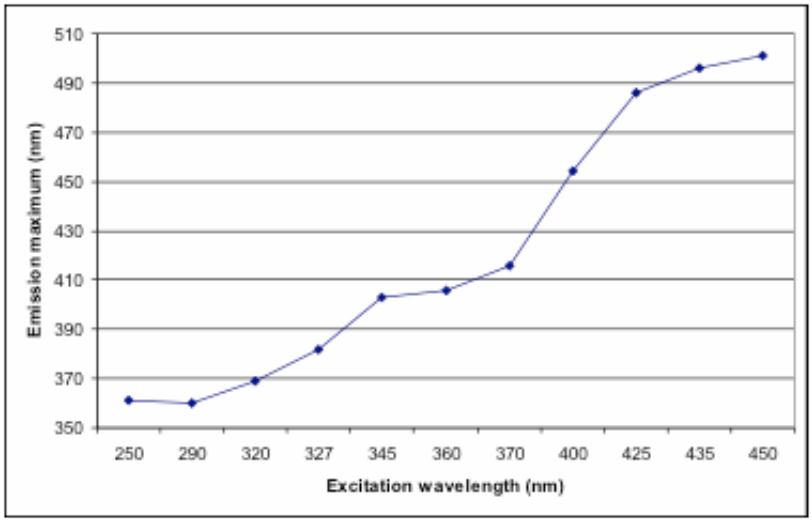

Figure S11. Variation of emission maximum of **3'** with excitation wavelength (MeOH).

Table S1. Excited states of **(N-Me 3')**.
First line reports PCM simulation of acetonitrile, second line methanol, third line dichloromethane.

No	Multiplicity	λ (nm)	f (au)	Orbitals [a]
1	Triplet	429 429 433	0.00	HOMO – LUMO
2	Triplet	403 403 405	0.00	HOMO – LUMO+1 HOMO-3 – LUMO
3	Singlet	352 352 357	0.11 0.10 0.11	HOMO – LUMO
4	Triplet	349 347 347	0.00	HOMO – LUMO+2 HOMO-3 – LUMO+1
5	Triplet	340 340 343	0.00	HOMO-1 – LUMO HOMO – LUMO+1
6	Triplet	339 338 339	0.00	HOMO – LUMO+2
7	Triplet	333 333 335	0.00	HOMO-1 – LUMO
8	Singlet	332 332 336	0.00	HOMO-1 – LUMO
9	Singlet	328 329 333	0.07 0.07 0.07	HOMO – LUMO+1
10	Triplet	321 321 324	0.00	HOMO-2 – LUMO
11	Singlet	318 318 318	0.01 0.01 0.02	HOMO – LUMO+2
12	Singlet	314 314 317	0.03 0.03 0.02	HOMO-2 – LUMO
13	Triplet	312 312 312	0.00	HOMO-1 – LUMO+2
14	Triplet	306 307 309	0.00	HOMO-1 – LUMO+1

15	Triplet	303 303 303	0.00	HOMO – LUMO+3
16	Singlet	302 302 306	0.01 0.01 0.01	HOMO-1 – LUMO+1
17	Triplet	301 301 302	0.00	HOMO-2 – LUMO+2 HOMO-1 – LUMO+1
18	Triplet	292 292 296	0.00	HOMO-2 – LUMO+1
19	Singlet	291 291 294	0.00 0.00 0.01	HOMO-1 – LUMO+2
20	Triplet	291 290 291	0.00	HOMO – LUMO+4

[a] Dominant contribution(s) are reported

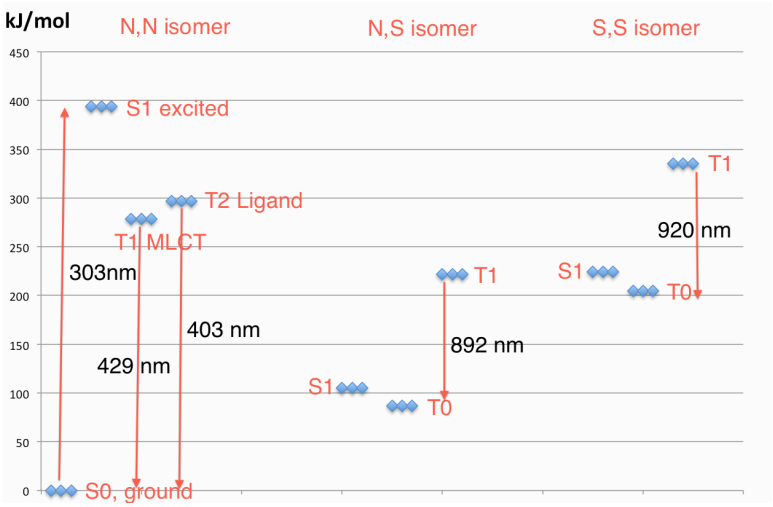

Figure S12. Summary of the relative energies of ground and excited states of **3'**.

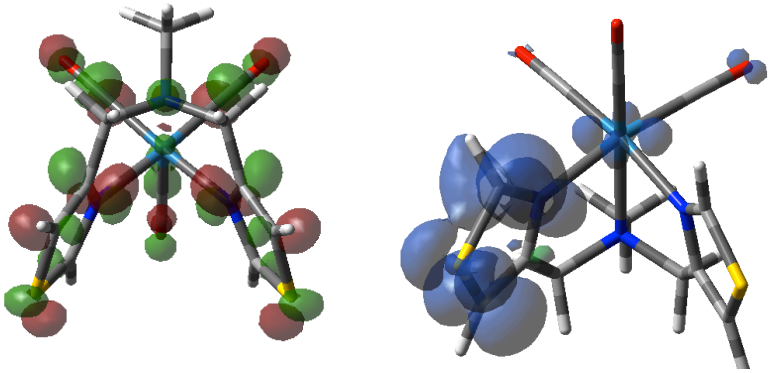

Figure S13. LUMO 3+ (left) and spin at triplet.

Table S2. Electronic absorption bands of **3'**.

Wavelength (nm)	**Assignment**	**A (m^2 mol^{-1}x 10^3)**
525 (shoulder)	^{1}MLCT	0.015
262	^{1}IL	4.5
235	^{1}IL	4.9

Table S3. Variation of emission maximum as a function of excitation wavelength for **3'**.

Solvent	DCM			MeCN			MeOH		
λ excitation nm (cm^{-1})	Emission λ max nm (cm^{-1})	Position of shoulder (if present) (nm)	Stokes shift (nm)	Emission λ max nm (cm^{-1})	Position of shoulder (if present) (nm)	Stokes shift (nm)	Emission λ max nm (cm^{-1})	Position of shoulder (if present) nm	Stokes shift (nm)
250 (40000)	361 (2770)		111	400 (25000)	356	150	399 (25062)		149
290 (34482)	360 (2777)		70	345 (28985)		55	389 (25706)		99
320 (31250)	369 (2710)		49	394 (25380)		74	399 (25062)		79
327 (30581)	382 (2617)		55	394 (25380)		67	399 (25062)		72
345 (28985)	403 (2481)	385	58	399 (25062)		54	405 (24691)	385	60
360 (27777)	406 (2463)	390	46	408 (24509)		48	443 (22573)	390	83
370 (27027)	416 (2403)	405	46	420 (23809)		50	419 (23866)	405	49
400 (25000)	454 (2202)	435	54	476 (21008)	458	76	485 (20618)	435	85
425 (23529)	486 (2057)		61	491 (20366)	473	66	529 (18903)		104
435 (22988)	496 (2016)	485	61	504 (19841)	485	69	543 (18416)	485	108

450 (22222)	501 (1996)	525	51	522 (19157)	502	72	551 (18148)	525	101

Table S4. Variation of Quantum Yield as a function of excitation wavelength for **3'**(MeOH).

Excitation wavelength (nm)	**Emission Maximum (nm)**	**Q (x 10^3)**
320	369	2.9
370	416	6.1
400	454	3.6

Table S5. Variation of lifetime as a function of excitation wavelength for **3'** (MeOH).

Excitation wavelength (nm)	**Emission Detection (nm)**	**τ (ns) (major component)**
295	370	0.9
372	450	4.9

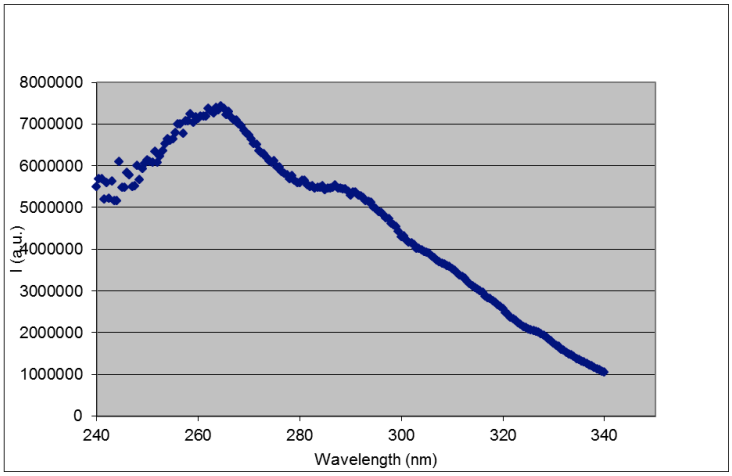

Figure S14. Excitation spectrum of **3'** (MeOH). Detection 360 nm.

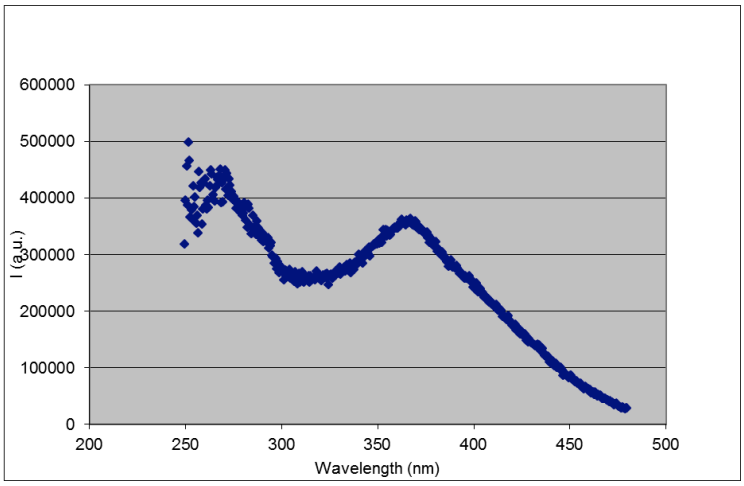

Figure S15. Excitation spectrum of **3'** (MeOH). Detection at 500 nm.

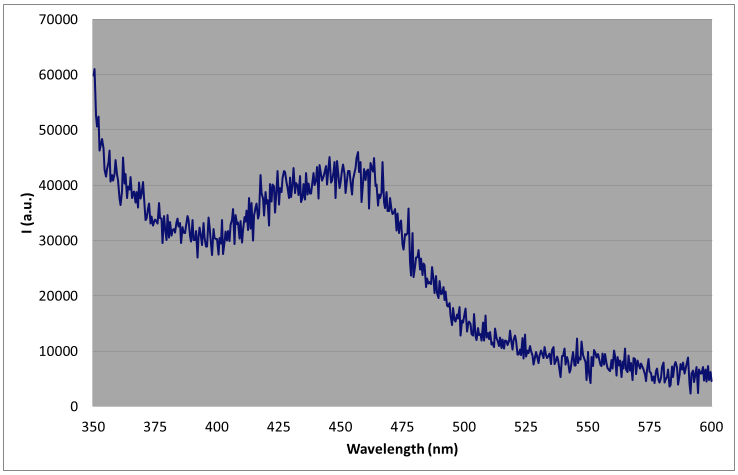

Figure S16. Excitation spectrum of **3'** (MeOH). Detection at 688 nm.

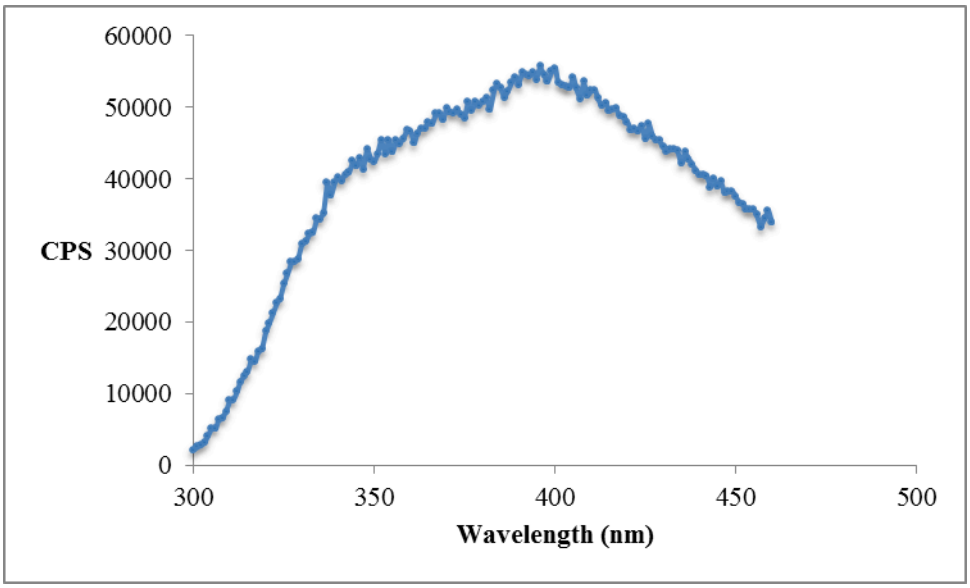

Figure S17. Emission spectrum of **3'** via excitation at 250 nm (MeCN).

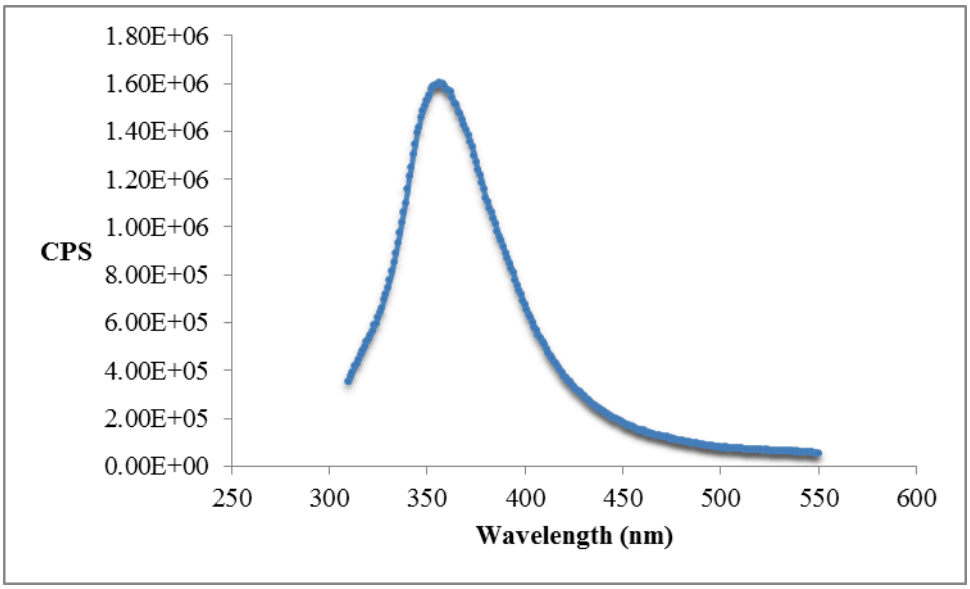

Figure S18. Emission spectrum of **3'** via excitation at 290 nm (MeCN).

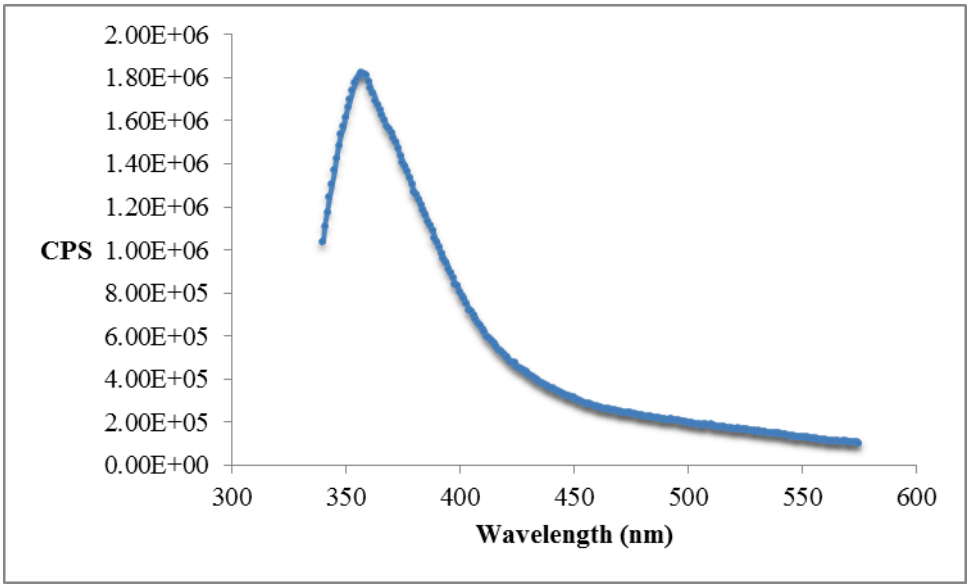

Figure S19. Emission spectrum of **3'** via excitation at 320 nm (MeCN).

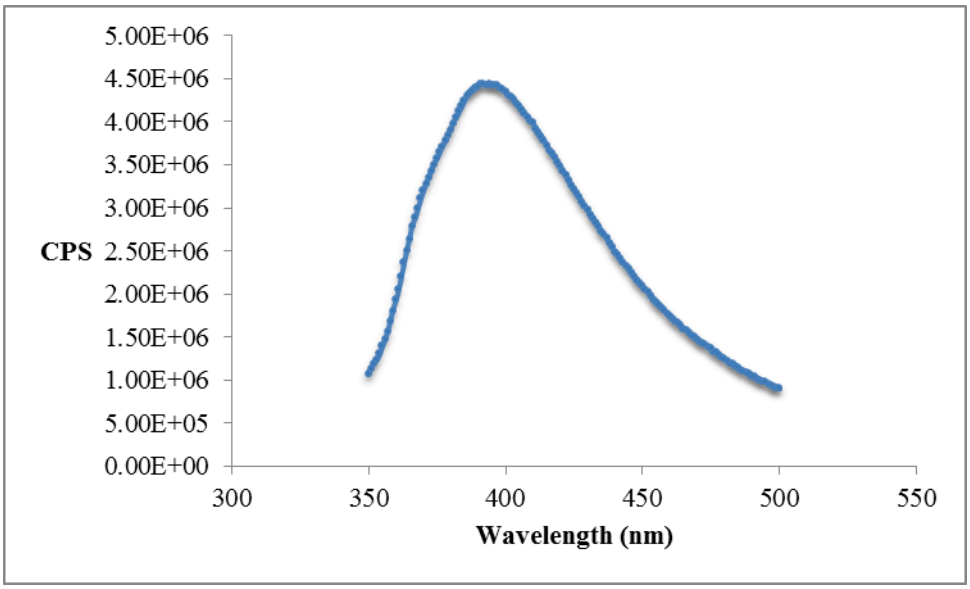

Figure S20. Emission spectrum of **3'** via excitation at 327 nm (MeCN).

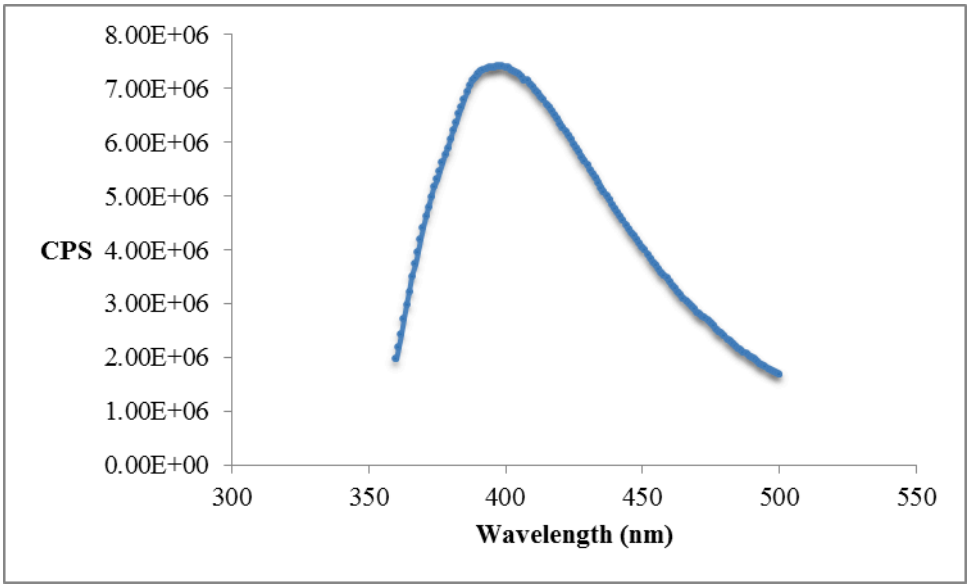

Figure S21. Emission spectrum of **3'** via excitation at 345 nm (MeCN).

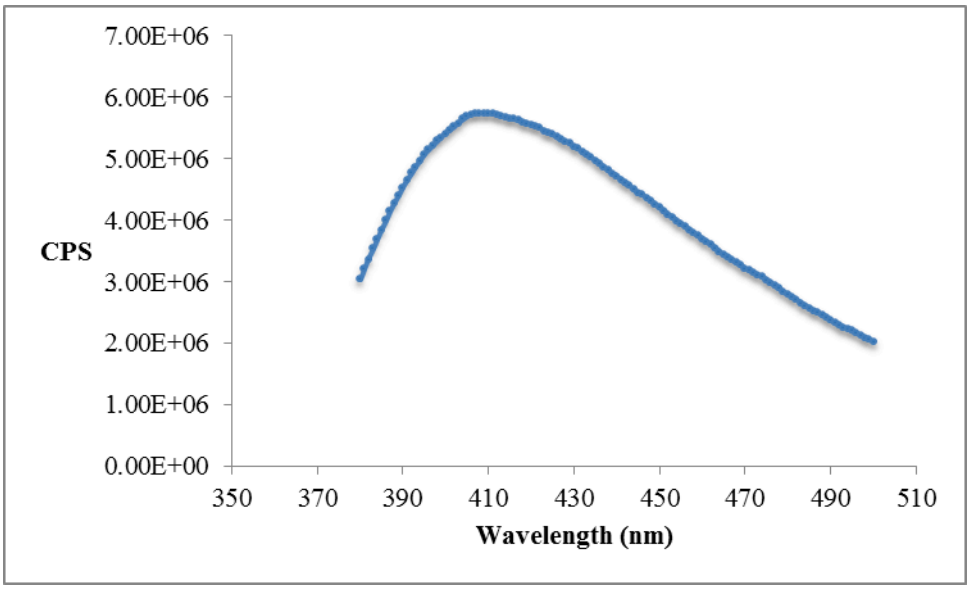

Figure S22. Emission spectrum of **3'** via excitation at 360 nm (MeCN).

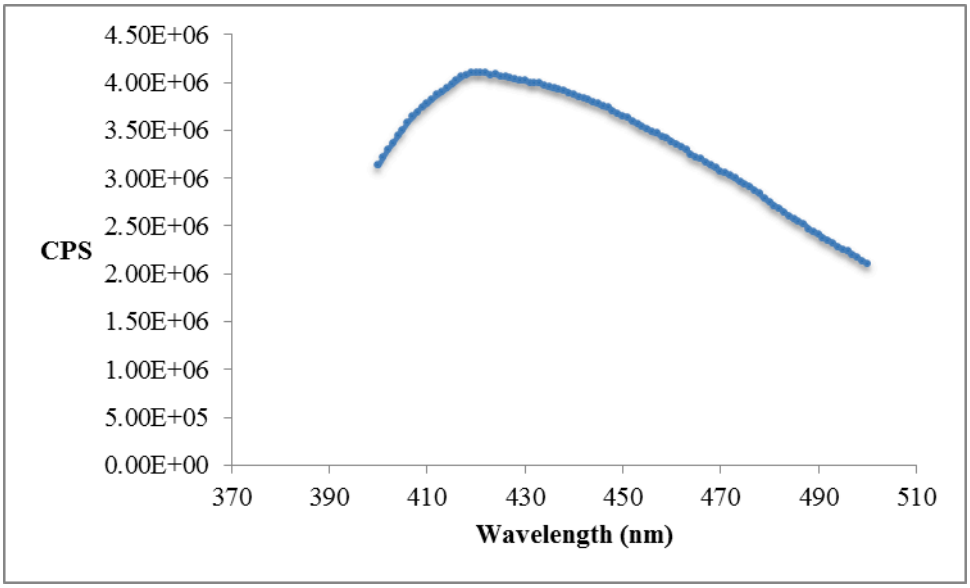

Figure S23. Emission spectrum of **3'** via excitation at 370 nm (MeCN).

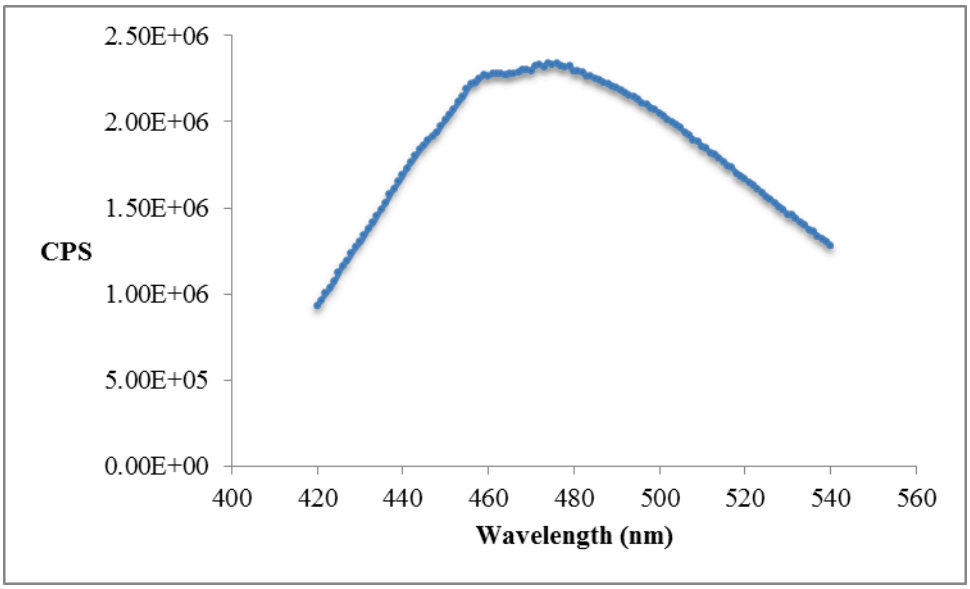

Figure S24. Emission spectrum of **3'** via excitation at 400 nm (MeCN).

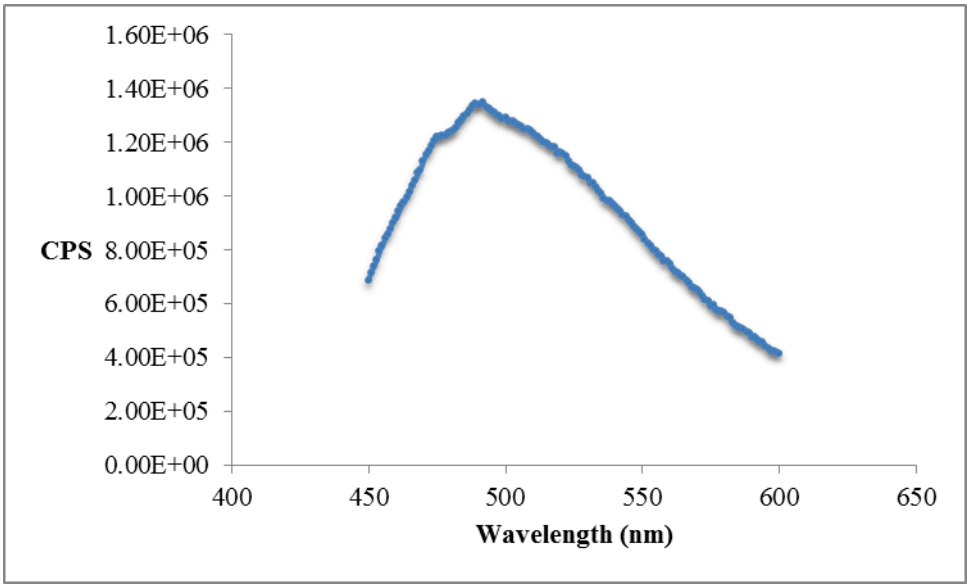

Figure S25. Emission spectrum of **3'** via excitation at 425 nm (MeCN).

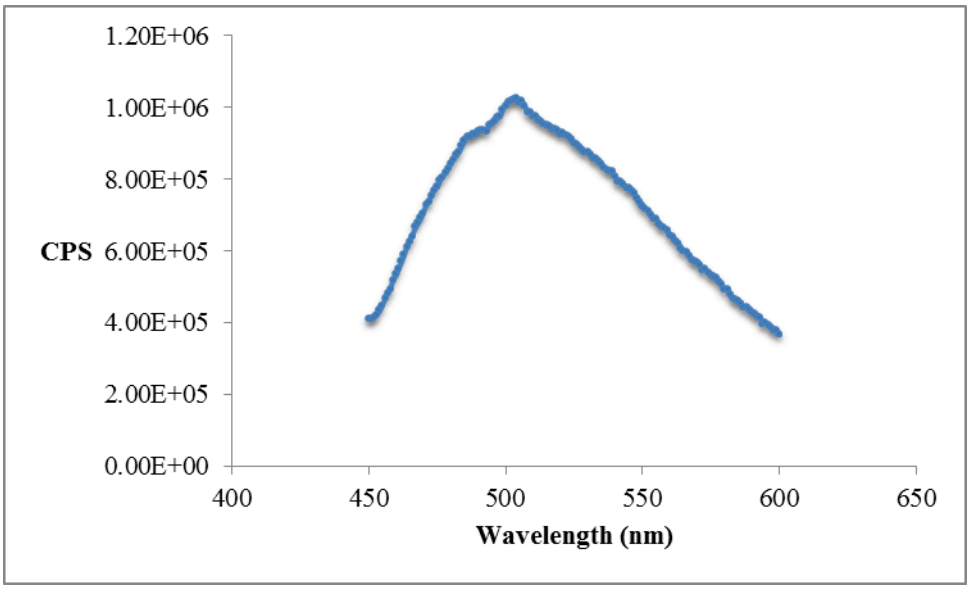

Figure S26. Emission spectrum of **3'** via excitation at 435 nm (MeCN).

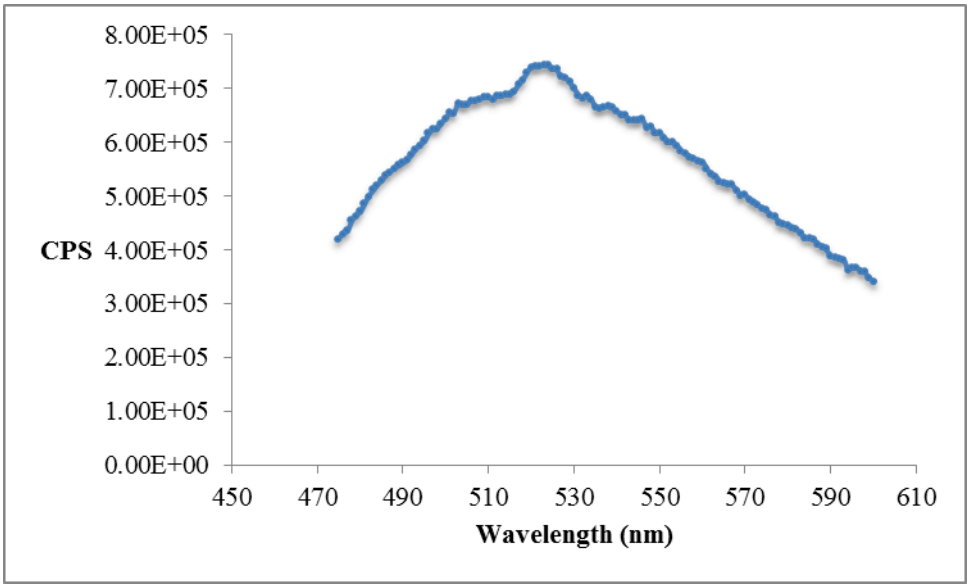

Figure S27. Emission spectrum of **3'** via excitation at 450 nm (MeCN).

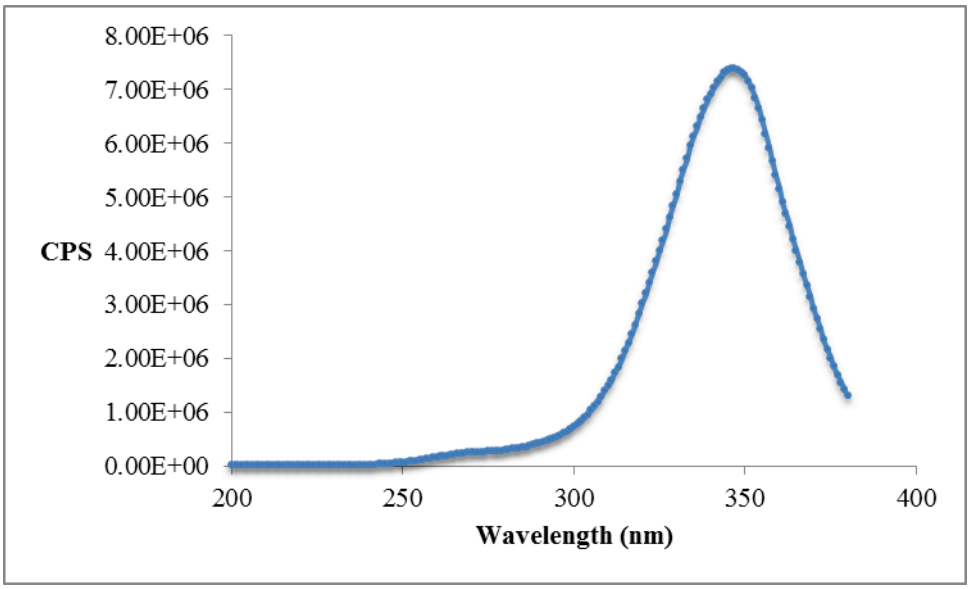

Figure S28. Excitation spectrum of **3'** (MeCN). Detection at 400 nm

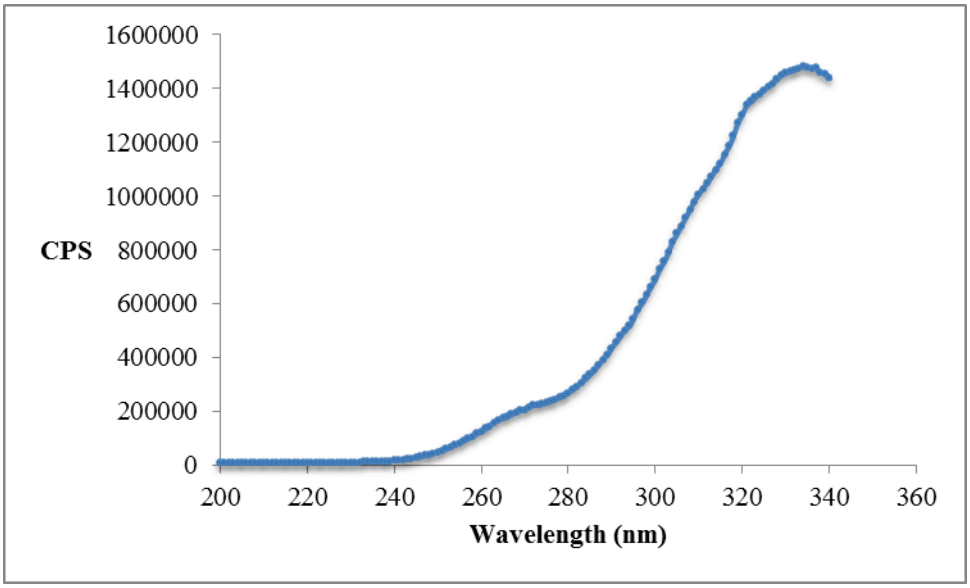

Figure S29. Excitation spectrum of **3'** (MeCN). Detection at 345 nm.

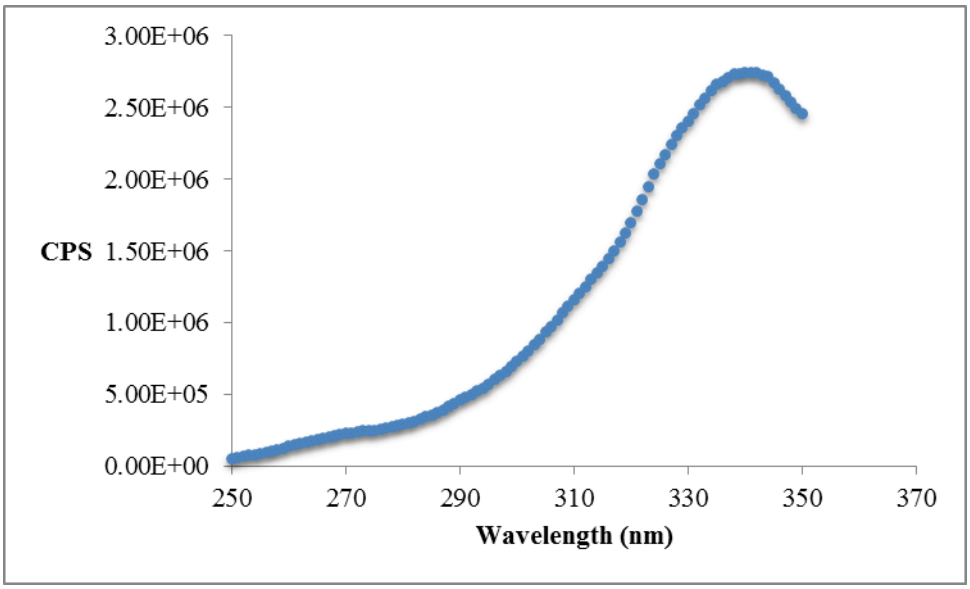

Figure S30. Excitation spectrum of **3'** (MeCN). Detection at 394 nm.

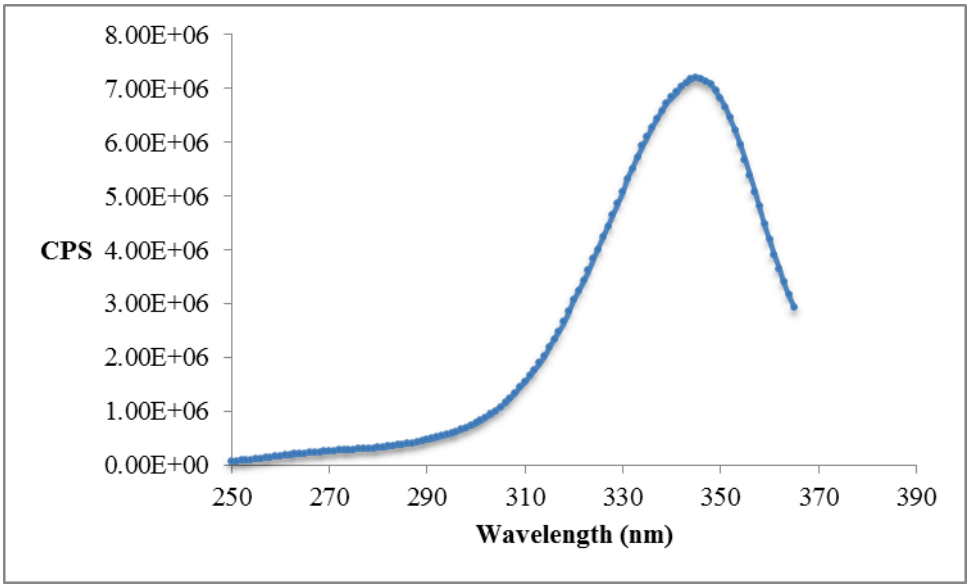

Figure S31. Excitation spectrum of **3'** (MeCN). Detection at 399 nm.

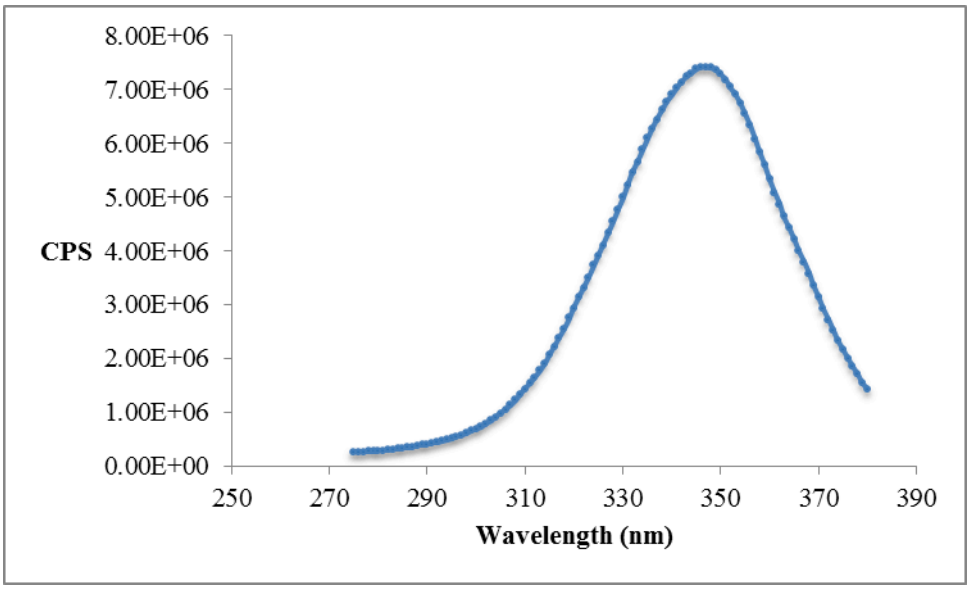

Figure S32. Excitation spectrum of **3'** (MeCN). Detection at 408 nm.

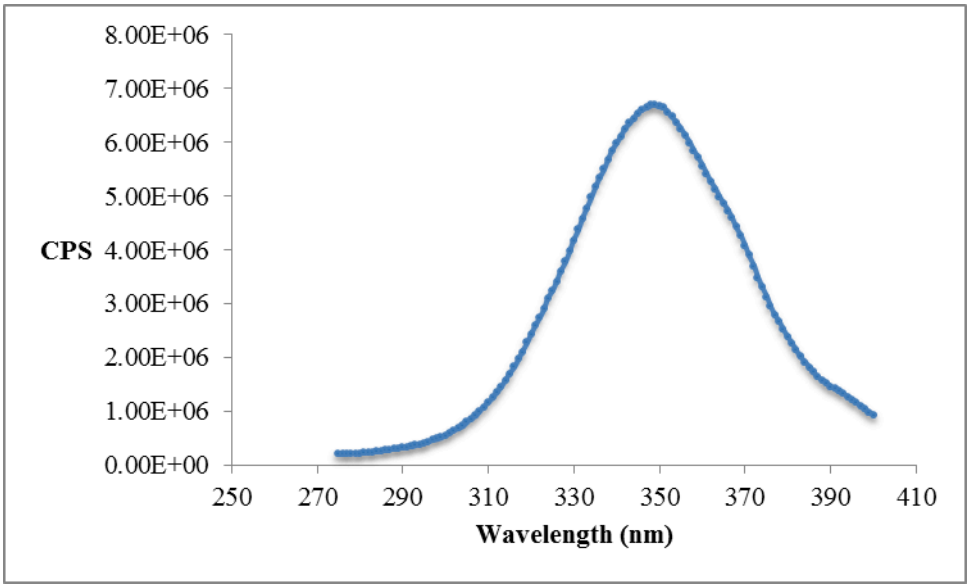

Figure S33. Excitation spectrum of **3'** (MeCN). Detection at 420 nm.

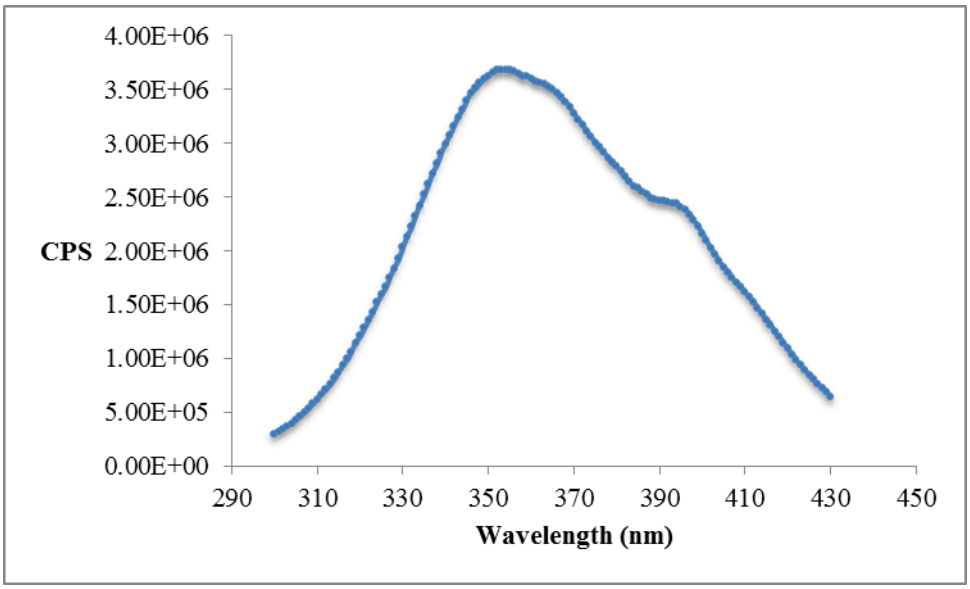

Figure S34. Excitation spectrum of **3'** (MeCN). Detection at 476 nm.

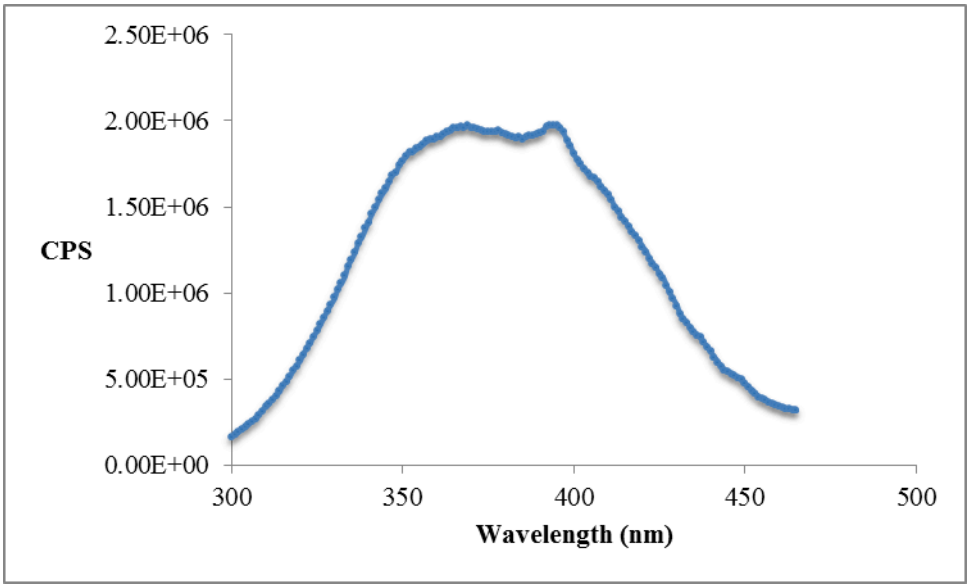

Figure S35. Excitation spectrum of **3'** (MeCN). Detection at 491 nm.

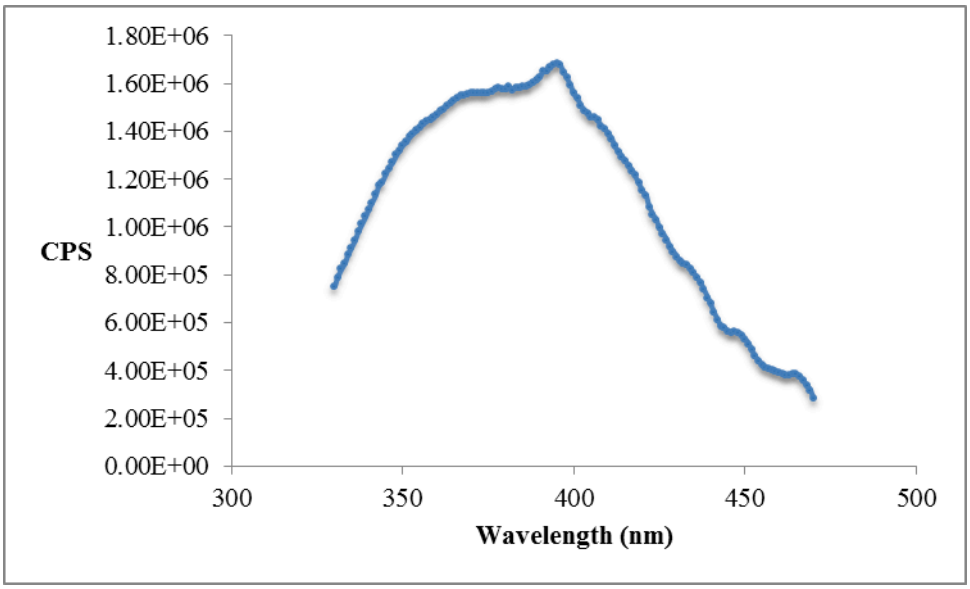

Figure S36. Excitation spectrum of **3'** (MeCN). Detection at 504 nm.

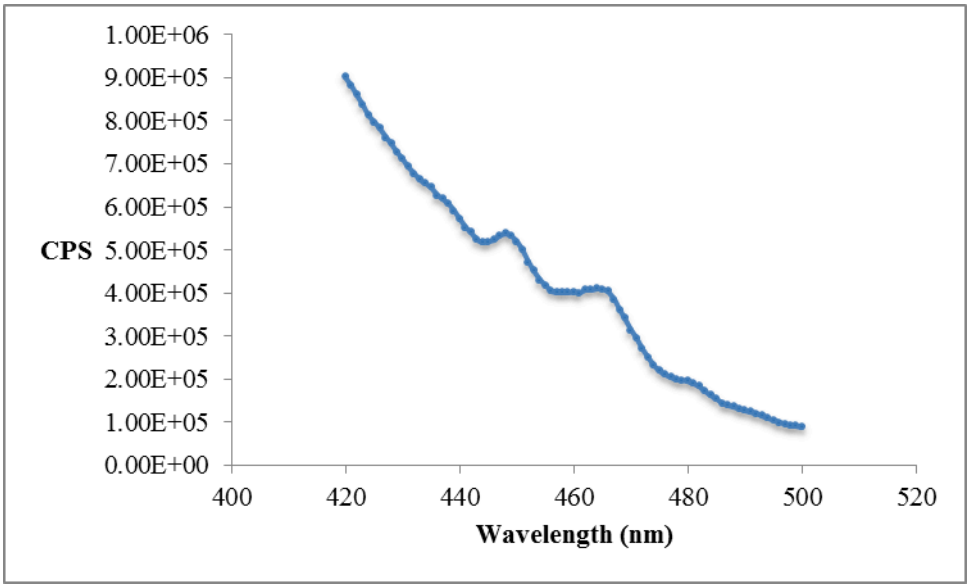

Figure S37. Excitation spectrum of **3'** (MeCN). Detection at 522 nm.

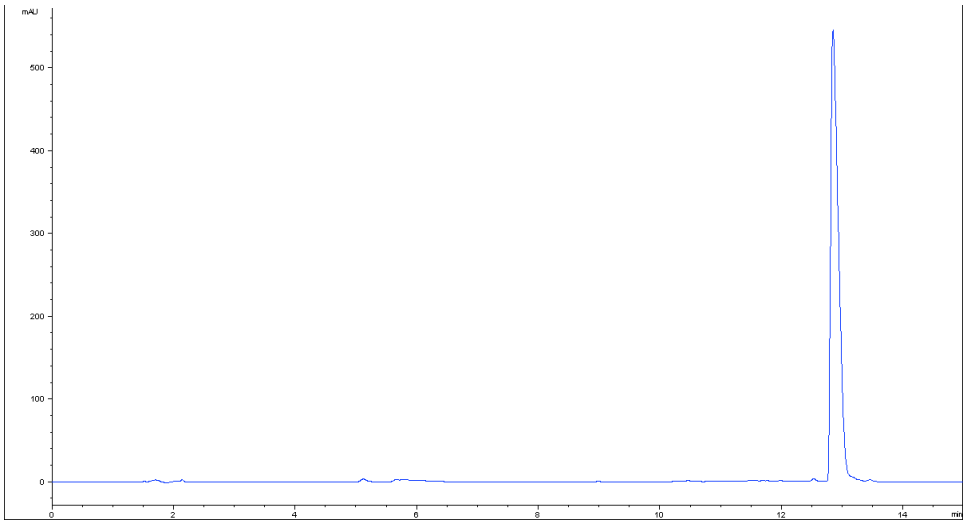

Figure S38. Chromatogram of **3'**; the peak at t_R 13 minutes represents complex **3'** post irradiation in MeCN (UV 254 nm). No change was observed in purity or speciation as compared to Figure S5.

1. Gaussian 03, Revision D.01, M. J. Frisch *et al*., Gaussian, Inc., Wallingford CT, 2004.
2. Gaussian09 Rev C.01, M. J. Frisch *et al*., Gaussian, Inc., Wallingford CT, 2010.
3. a) A. D. Becke, J. Chem. Phys., 98 (1993) 5648-52. b) C. Lee, W. Yang, R. G. Parr, Phys. Rev. B, 37 (1988) 785-89.
4. P. J. Hay and W. R. Wadt, J. Chem. Phys., 82 (1985) 270-83.
5. a) R. Ditchfield, W. J. Hehre, and J. A. Pople, J. Chem. Phys., 54 (1971) 724. b) P. C. Hariharan and J. A. Pople, Theor. Chem. Acc., 28 (1973) 213-22. C) M. M. Francl, W. J. Pietro, W. J. Hehre, J. S. Binkley, D. J. DeFrees, J. A. Pople, and M. S. Gordon, J. Chem. Phys., 77 (1982) 3654-65. d) T. Clark, J. Chandrasekhar, G. W. Spitznagel, and P. v. R. Schleyer, J. Comp. Chem., 4 (1983) 294-301.
6. D. Andrae, U. Haeussermann, M. Dolg, H. Stoll, and H. Preuss, Theor. Chem. Acc., 77 (1990) 123-41.
7. J. Tomasi, B. Mennucci, and R. Cammi, Chem. Rev., 105 (2005) 2999-3093.